# Ultrasonic Elasticity Imaging as a Tool for Breast Cancer Diagnosis and Research



Claire Pellot-Barakat[1,2], Mallika Sridhar[1], Karen K. Lindfors[3], Michael F. Insana[1,4,*]

[1]*Department of Biomedical Engineering, University of California, Davis CA,* [2]*INSERM UMR-S 678, Paris, France,* [3]*Radiology Department, University of California, Davis, Sacramento CA,* [4]*Department of Bioengineering, University of Illinois at Urbana-Champaign, Urbana IL*

**Abstract:** Ultrasonic elasticity imaging is a promising new tool for breast cancer diagnosis and management. Ultrasound is applied to sense small local tissue deformations noninvasively to image stiffness and thus exploit the large intrinsic stiffness contrast generated during the progression of many diseases *in vivo*. This paper briefly reviews several related approaches to breast elasticity imaging to explain some of the observed variability in breast imaging results. Preliminary clinical results from a population of 13 patients with small and nonpalpable breast lesions obtained with a low noise elasticity imaging algorithm developed in our group are then reported. All the benign lesions exhibited normal elasticity ranges. About half of the malignant lesions were undetected with elasticity imaging most likely because of their small size (<7mm) or softening from the addition of fatty-replaced tissue. Other malignant lesions were clearly identified as areas with extreme elasticity values compared to their surroundings. We observed that some malignant lesions did not exhibit any desmoplasic stiffening while others showed an uncommon softening. It is clear that by broadening the study population to include small and nonpalpable lesions, we see much variability in elasticity image findings.

**Keywords:** Desmoplasia, palpation, strain imaging, tumor metabolism, ultrasound.

## I- INTRODUCTION

Breast cancer is the most common cancer among women in western countries. In the United States, the risk for a woman to develop a breast cancer in her lifetime is 1 in 7 [1]. Early diagnosis and treatment of breast cancer are essential to decrease breast cancer-related mortality [2]. Until now, breast cancer diagnosis has been based mainly on information from clinical examinations combined with anatomical imaging, such as x-ray mammography or sonography, where the tumor visibility depends on nonspecific contrast mechanisms. Studies have shown that the sensitivity of mammography increases with age: mammography is particularly sensitive for older women with fatty replaced breast tissue, but has a lower sensitivity in young women with dense breasts. On the contrary, sonography has in general a higher sensitivity in women with dense breasts [3]. The integration of mammography and sonography in clinical practice has a sensitivity of 89-92% in detection of cancer [4]. However, less than one in three lesions identified as suspicious by these combined techniques is actually malignant. Thus, a large number of benign biopsies are carried out that result in anxiety, discomfort, risk of infection, and additional medical expenses. These biopsies would not be necessary if benign lesions could be differentiated from cancerous tumors by specific and noninvasive procedures used complementarily to standard imaging procedures.

In order to improve diagnostic specificity and prognostic indicators for breast cancer, current trends in cancer imaging aim to develop techniques that directly image molecular signaling mechanisms among tumor cells. Such signaling among epithelial, inflammatory and stromal tumor cells is a critical process guiding the growth and progression of breast carcinomas [5]. Molecular imaging techniques that access tumor biology, in particular tumor perfusion imaging, are being developed in MRI [6], PET [7] or optical imaging techniques [8]. Although these techniques are promising, they have issues of toxicity, biodistribution, specificity and cost. Elasticity imaging is an emerging technique for breast cancer diagnosis and management that can directly and noninvasively image the effects of molecular signaling processes in disease mechanisms *in vivo* and provide specific information on alterations of breast tissue structures. Ultrasound and MRI techniques are used to detect small local tissue deformations that reflect elasticity. The large intrinsic stiffness contrast generated by most pathological tissue can be exploited in elasticity imaging [9-14]. Furthermore, time-varying mechanical features of breast tissues [15-17] could provide information about the tissue microenvironment that affects molecular signaling and controls the rate of tumor growth, metastatic potential, and response to therapy [18]. Elasticity imaging is hence being developed not only as a tool for clinical diagnosis but also potentially for basic biological research.

An initial clinical study by Garra in 1997 [9] demonstrated the ability of ultrasonic elasticity imaging to aid in the detection and classification of lesions. A recent ultrasonic elastography study by Hall *et al*. [12] including 29 patients showed significant changes in elasticity in cases of fibroadenoma, cysts and carcinomas. Malignant lesions appeared consistently stiffer than their surrounding tissue. They also appeared two to three times larger on elastograms than on sonograms while benign lesions tended to have

*Address correspondence to this author at the Department of Bioengineering, University of Illinois at Urbana Champaign, Urbana, IL 61801; Tel: (217) 333-1867; Fax: (217) 265-0246; E-mail: mfi@uiuc.edu

**1573-4056/06 $50.00+.00** 

about the same size on both images. The size difference was attributed to desmoplasia which is a dense collagenous stroma that stiffens malignant palpable tumors [19]. This desmoplastic reaction of malignant breast tumors was described by Garra [9] as a distinctive feature of elasticity images useful for differential diagnosis. Hiltawsky *et al.* [11] also found significant differences in strain between solid lesions (defined as cancerous lesions and benign lesions except for fibrous mastopathy) but were not able to show from ultrasonic elastograms alone that it was possible to distinguish benign from malignant lesions in general. Other groups working with magnetic resonance elastography (MRE) methods found malignant lesions to be twice as stiff as benign lesions [13] and malignancies more than four times stiffer than the surrounding parenchymal tissue [14]. MR allows data acquisition from a finely-sampled tissue volume, which is ideal for imaging complex 3D deformations, while ultrasound currently is limited to imaging deformation in a plane. However ultrasound often provides higher temporal resolution for acquisition, and therefore allows tracking of fast, non-repetitive physiological deformations. It also has the advantage of being inexpensive, widely available and easily extendable to viscoelasticity imaging. This paper focuses on ultrasonic elasticity imaging.

Breast ultrasonic elasticity imaging studies reported so far in the literature have mostly concerned large (>15mm) and palpable lesions. We are expanding the examined patient population to include small, nonpalpable breast lesions, which requires that we suppress decorrelation noise to see these lower contrast lesions. For this application we developed a high resolution algorithm that is based on a priori knowledge of tissue mechanics and is robust to noise [20], and we tested it clinically on a population of 13 patients with nonpalpable breast lesions ranging in size from 0.5 to 2 cm. The method is now being extended so that we can also image the viscoelastic behavior of tissue, thus adding time-varying mechanical properties of tissue to the assessment.

## II- BREAST ELASTICITY IMAGING TECHNIQUES

### Tissue Deformation

Elasticity imaging can be performed using either static or dynamic mechanical stimuli. Static and dynamic techniques provide different features of the material properties of tissue. Static elasticity imaging techniques assess elastic properties of tissues by applying and holding a steady mechanical force [20-23]. With ultrasound, the tissue can be compressed by applying a pressure with the transducer. Radio-frequency (RF) data are recorded before and after the sudden force application, and the elastic strain is estimated either immediately before viscous responses can engage or after a long delay that allows the viscous flows to settle. In dynamic imaging, a stress field that varies periodically over time is applied while tracking movements ultrasonically [24]. Ultrasound techniques using acoustic radiation force to apply a local impulse stress stimuli were recently developed by Nightingale *et al*. [15]. Harmonic stimuli coupled with very fast frame rate acquisition (6 Kframes/sec) have also been applied by Fink's group to image moving shear waves that can be used to visualize viscoelastic properties of tissue [16]. While both of these methods have significant potential for providing unique biophysical information about disease, they require major modifications to current instrumentation or risky high intensity sound pulses to implement.

We have shown for the first time [17] that simple step- or ramp-compression stimuli combined with timed RF acquisitions can produce a time series of strain images that describe the spatial distribution of tissue elasticity as well as the viscous strain decay, which could eventually be used to track changes in stromal tissues that describe important features of malignant breast disease. The tissue deformation immediately resulting from the step compression is directly related to the elastic strain while the time-varying response depends on the viscous relaxation time constants. This method has the advantages of requiring no injectable contrast media or high-intensity pulse transmissions.

In clinical ultrasound applications, tissue deformation is generated by freehand compression of the tissue with the transducer for ease of use and convenience. Freehand imaging poses several problems, in particular tissue motion that is out of the imaging plane results in echo decorrelation and strain noise that obliterates most image features. We can avoid echo decorrelation by acquiring echoes from a highly sampled volume of tissue, as is common with MRE approaches. However techniques that offer high-speed 4-D ultrasonic acquisition are still under development. When limited to 2-D echo acquisition, it is thus important to use a strain algorithm that is robust to echo decorrelation.

### Strain Estimation

Strain images are usually obtained by computing the derivative of tissue displacement occurring along the axis of the ultrasound beam. To estimate displacement, most techniques involve cross-correlation analysis or block matching algorithms based on Sum Absolute Differences (SAD) or Sum Squared Differences (SSD) [21, 26-28].

These estimators are particularly accurate and efficient for tracking small motion. However, incoherent motion and variations in the echo signal amplitude lead to ambiguities in the determination of the displacement when only RF data information is used. Such ambiguities are resolved by applying appropriate a priori knowledge of tissue mechanical properties into the motion estimation process. For that purpose, we developed a strain estimation algorithm based on a regularization of the optical flow (OF) constraint. The OF constraint assumes the conservation of intensity through motion [20]. The proposed regularized optical flow (ROF) algorithm estimates the most probable value of the displacement field $d$ by minimizing a global cost function that reflects the typical constraint of conservation of echo amplitude while imposing a smoothness constraint on the displacement field:

$$\hat{d} = \arg\min_{d}(E_e(d) + \alpha E_s(d)).$$

In this simplified notation, the function argmin returns the displacement field $d$ as the estimate $\hat{d}$ that minimizes the sum of energy functions $(E_e(d)+ \alpha E_s(d))$. $E_e$ is the accumulated difference between the echo signals acquired before and after tissue deformation, $E_s$ is the accumulated difference between a given point in the image and its neighbors and $\alpha$ is a constant, called regularization

parameter. The latter term forces the image to be smooth, which we know a priori to be generally true of breast tissue deformations. The displacement estimate then is a balance between information obtained from the acquired compression data $E_e$ and a priori knowledge that deformations are spatially smooth $E_s$; $\alpha$ sets the balance. For in-plane tissue motion and low-noise echo data, $\alpha$ is set to a small value, and we rely more on the experimental data and less on the prior. The best value of $\alpha$ has been shown to be 2.5 [20]. This approach is commonly used for image reconstructions from noisy data [29].

Performances of the regularized algorithm in terms of contrast, noise and resolution were evaluated and compared to that of a multi-resolution cross-correlation based method (MRCC) using data from a gelatin phantom [30]. The MRCC algorithm is based on a maximization of the cross-correlation of echo amplitudes only, which is a direct measure that does not require any iterative process since it is based entirely on the data, while the ROF method performs a compromise between echo amplitude conservation and smoothness of displacement field, which requires an iterative procedure during which estimates are refined. The MRCC is thus accurate in perfectly coherent data, i.e., all echo signals in the pre-deformation echo frame can be found undistorted in the post-deformation echo frame. However the MRCC algorithm is highly susceptible to decorrelation noise as echo coherence is lost.

The comparative measurements of contrast and noise performances between the ROF and MRCC methods indicated that the regularization strongly improves noise characteristics while preserving lesion contrast and spatial resolution. To illustrate these methods, we show a B-scan of a soft flow channel phantom with a stiff cylindrical inclusion acquired before compression in Fig. (**1a**). In Figs. (**1b**) and (**1c**) we show the elastograms of the phantom corresponding to an applied 3% strain[1] obtained with the MRCC and ROF algorithms respectively. The gray scale bar indicates percent strain, where positive values are compressive and negative values are tensile. The stiff inclusion appears dark (low strain) while the soft flow channel appears bright (high strain). The general appearance of the ROF elastogram is smoother than that of the MRCC elastogram, and the decorrelation around the channel is minimal. The smoothing effect of the ROF algorithm intervenes mainly in ambiguous regions of large motion transitions with high decorrelation noise (such as around the soft channel). High resolution and contrast characteristics are maintained in non-decorrelated regions. However, in case of freehand acquired breast data, the roughness penalty in the regularized algorithm can also lead to over smoothing of regions that are decorrelated due to out-of-plane compression, resulting in a loss of spatial resolution and image contrast in these regions. Although the ROF algorithm consistently provides lower noise strain images, the two methods thus have complementary strengths under the heterogeneous elasticity conditions common to breast imaging.

[1] If the object height is $L$ before deformation and $L'$ after deformation, then the applied percent strain is $100 \times (L - L') / L$.

## Proposed Analysis Protocol

There is always a risk of using prior information that may not apply to all areas of an image. To ensure that the ROF algorithm reduces decorrelation noise without producing artifacts, we reconstructed strain images using both the MRCC and ROF algorithms and compared the results.

Since the information used in the MRCC approach is just a part of that used in the ROF approach, it seems reasonable to assume that an agreement between the MRCC and ROF strain images indicates that the estimates are not degraded by processing artifacts arising from the smoothness constraint. Furthermore, as mentioned in the previous paragraph, the two formed strain images can be used in a complementary way to provide a more confident interpretation of observed strain patterns. Controlling for processing artifacts, the only factor affecting the strain results is the compression itself, whose quality can be controlled by a very carefully applied acquisition protocol.

Another feature of our protocol is our analysis of the displacement map together with the strain image. Although the two images are related (strain is the spatial derivative of displacement), lesion contrast can be very different. Different representations of the same information can thus highlight features in some regions that otherwise are lost by lack of contrast. They can also help us interpret image findings with respect to tissue changes. For illustration purposes, Fig. (**2**) shows the displacement maps corresponding to a homogeneous phantom and to the flow phantom shown on Fig. (**1a**) respectively. The color scale bar indicates displacement in mm. The further the tissue is from the transducer, the more it appears to be displaced. Thus there is a gradual increase in displacement from the top to the bottom of the map. In Fig. (**2b**), there is a large bulge due to smaller displacements from the stiff region. We should specify that in freehand *in vivo* elasticity imaging, the displacement map is not as simple to interpret as in phantom experiments with precise motion and boundary control. Occasionally, displacement increases more on one side than the other due to slippage of the tissue and not its material properties.

Although it is normally impractical to use all three images for clinical exams, we believe that it is important to use as much information as possible in the current phase of understanding observed elasticity patterns and finding a discriminative protocol.

## III- EARLY CLINICAL RESULTS

We selected a patient population different than the ones reported in the literature for our preliminary clinical study. These patients had suspicious masses discovered on screening mammograms that were nonpalpable. The diagnosis for each lesion was determined by ultrasound guided core biopsy performed just after our elasticity imaging exam.

A total of 13 patients are included in our study. The patients were all placed in the supine or oblique position with ipsilateral arm overhead and the breasts were compressed in the AP direction using the chest wall as a rigid boundary against which the compression is applied.

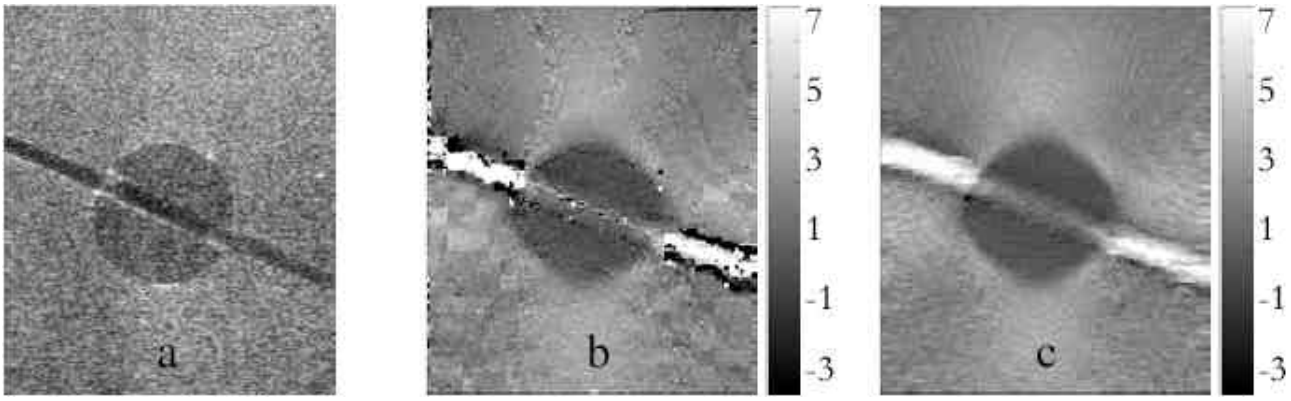


**Fig. (1).** a) B-mode of a gelatin phantom with a flow channel and stiff cylindrical inclusion, b) MRCC elastogram, c) ROF elastogram. The stiff inclusion has a low strain (appears dark on the elastogram) while the soft channel has a high strain (bright).

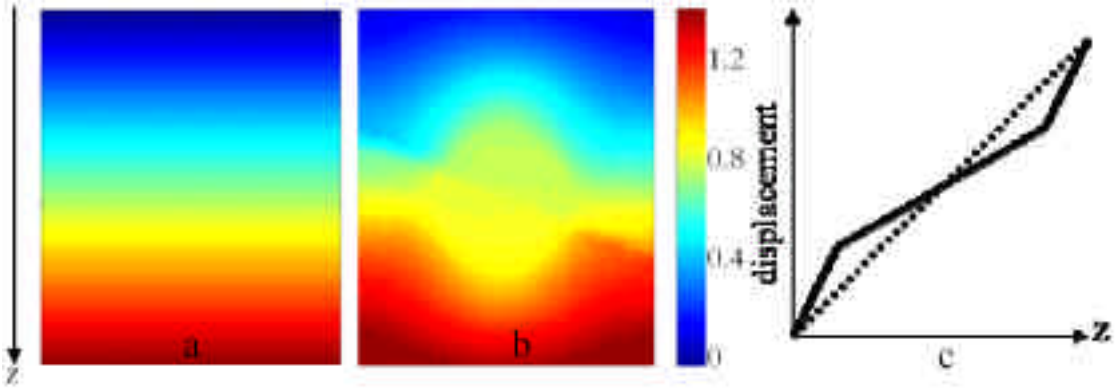


**Fig. (2).** Displacements maps of a) a homogeneous phantom, b) the phantom with a stiff inclusion (shown in Fig 1a), c) Displacement as function of depth profiles for the homogeneous phantom (dashed line) and the flow phantom (solid line).

Patient ages ranged from 46 to 83 years, and the lesion sizes ranged from 5 to 20 mm (Table **1**). The pathology reports obtained after biopsy indicated that 6 patients had benign lesions and 7 had malignant lesions. Results from two of these lesions were reported previously [18].

Multi-compression acquisition [31] was used to maximize strain contrast without incurring high decorrelation noise and also without compromising spatial resolution by relying totally on the regularization parameter to control decorrelation noise. The elastograms displayed were obtained by adding strain estimates from successive frames acquired during compression, each corresponding to a small compression of 0.15 to 0.3% for a total applied compression of 1.4 to 3.7 %. Table **1** summarizes the age distribution of the population studied, the lesion size and depth from the breast skin, the histopathological diagnosis and the elasticity findings. Good agreement was found between the two algorithms in all cases, with ROF elasticity images consistently providing the superior quality image. In the following, only ROF strain images are shown systematically. The displacement maps are shown whenever they reveal new information.

All the benign lesions in our study exhibited normal elasticity ranges, as expected for many benign masses. Among the 7 malignant lesions, 2 nonpalpable lesions were clearly detected as areas with extreme elasticity values compared to the surrounding tissue while 2 malignant lesions could not be identified with elasticity imaging. The 3 other malignant lesions did not exhibit very striking elasticity patterns but had suspiciously high or low displacements. These results are illustrated below.

Two sonographically suspicious, nonpalpable lesions typical in our experience are shown in Fig. (**3**) where sonograms (Figs. (**3a**), (**3c**)) and elasticity images (Figs. (**3b**), (**3d**)) are compared. The first was a 12 mm benign lesion. The second was a 16 mm malignant lesion. The total compression applied to the benign and malignant lesions was less than 2% of the breast thickness. The sonograms of both lesions show poorly defined hypoechoic lesions. The echogenicities of both lesions are similar, however only the benign lesion (stromal fibrosis) generates little detectable strain contrast (Fig. (**3b**)) thus indicating that it has a stiffness comparable to that of the surrounding tissue. The malignant lesion (invasive lobular carcinoma; ILC), in contrast, is larger on the elastogram than on the sonogram and stiffer than its background, thus indicating the presence of desmoplasia (Fig. (**3d**)). This is the only especially stiff lesion we observed in our limited study, probably because we limited our patient population to nonpalpable lesions.

**Table 1. Summary of Patient (Age) and Lesion (Size and Depth) Information, Histopathology Reports, Elasticity Image Formation (% Compression) and Findings (Strain (ε) Contrast)**

| Age (yrs) | Size (mm) | Depth (mm) | Biopsy Report | Cmp % | Elasticity contrast (lesion /background) | Fig Ref |
|---|---|---|---|---|---|---|
| 46 | 12 | 15 | Benign (Fibroadenoma) | 1.5 | No notable ε contrast | |
| 47 | 20 | 10 | Benign (Fibrocystic Changes) | | No notable ε contrast | |
| 47 | 11 | 15 | Benign (Fibrocystic Changes) | 2.25 | No notable ε contrast | |
| 47 | 6 | 13 | Benign (Fibrocystic Changes) | | No notable ε contrast | |
| 48 | 16 | 16 | Benign (Fibrocystic Changes) | 2 | No notable ε contrast | |
| 52 | 12 | 15 | Benign (Stromal Fibrosis) | 1.5 | No notable ε contrast | **3a-b** |
| 46 | 6 | 16 | Malignant (IDC) | | No notable ε contrast | |
| 48 | 10 | 8 | Malignant (IDC) | 1.4 | Very soft | **4a-c** |
| 53 | 5 | 11 | Malignant (IDC) | | Displacement Bulge | **6a-c** |
| 66 | 16 | 25 | Malignant (ILC) | 1.9 | Very stiff | **3c-d** |
| 74 | 5 | 18 | Malignant (IDC) | | Displacement Bulge | |
| 81 | 10 | 24 | Malignant (ILC) | | Displacement Bulge | |
| 83 | 10 | 12 | Malignant (IDC) | 3.7 | No notable ε contrast | 5a-c |

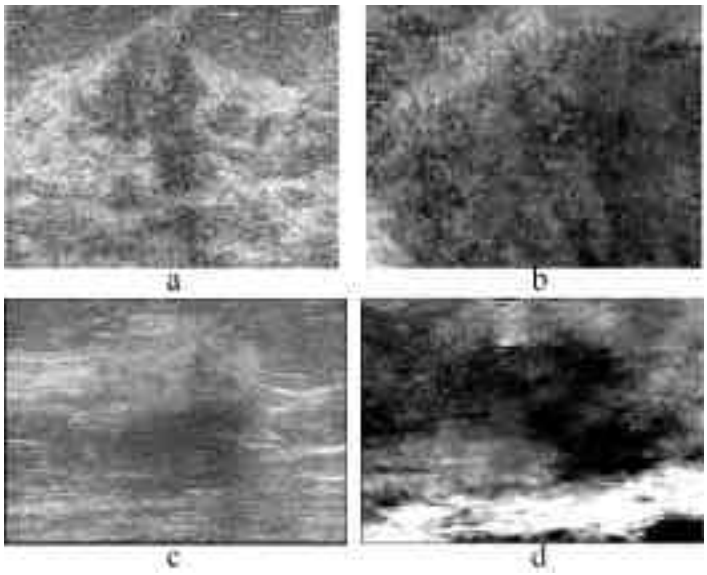


**Fig. (3).** Top row; sonogram (a) and elastogram (b) of a 12 mm lesion diagnosed as stromal fibrosis (52 yrs old patient). Bottom row; sonogram (c) and elastogram (d) of a 16 mm lesion diagnosed as invasive lobular carcinoma (66 yrs old patient).

Fig. (**4a**) shows a nonpalpable invasive ductal carcinoma (IDC). The 10 mm lesion appears much softer (brighter) than its surroundings on the elastogram (Fig. (**4c**)). The displacement map also clearly shows a region of excessive motion corresponding to very soft tissue (Fig. (**4b**)). The dark region mirrored below the bright region indicates negative strains, which gives the impression that the tissues are being stretched in this area. Soft malignant lesions are much less frequently observed than stiff ones. The histology of lesions has not yet been correlated with tissue mechanical properties. We conjecture that the soft appearance of the lesion may be due to factors related to the specific tumor histology and the surrounding tissue environment. For instance, some early stage non-palpable tumors like the above do not exhibit desmoplasia [32]. Additionally their metabolic requirements cause an upregulation of matrix metalloproteinase production, resulting in extracellular matrix breakdown to enable neovascularization [33]. Both these factors could result in soft lesions as seen in this case.

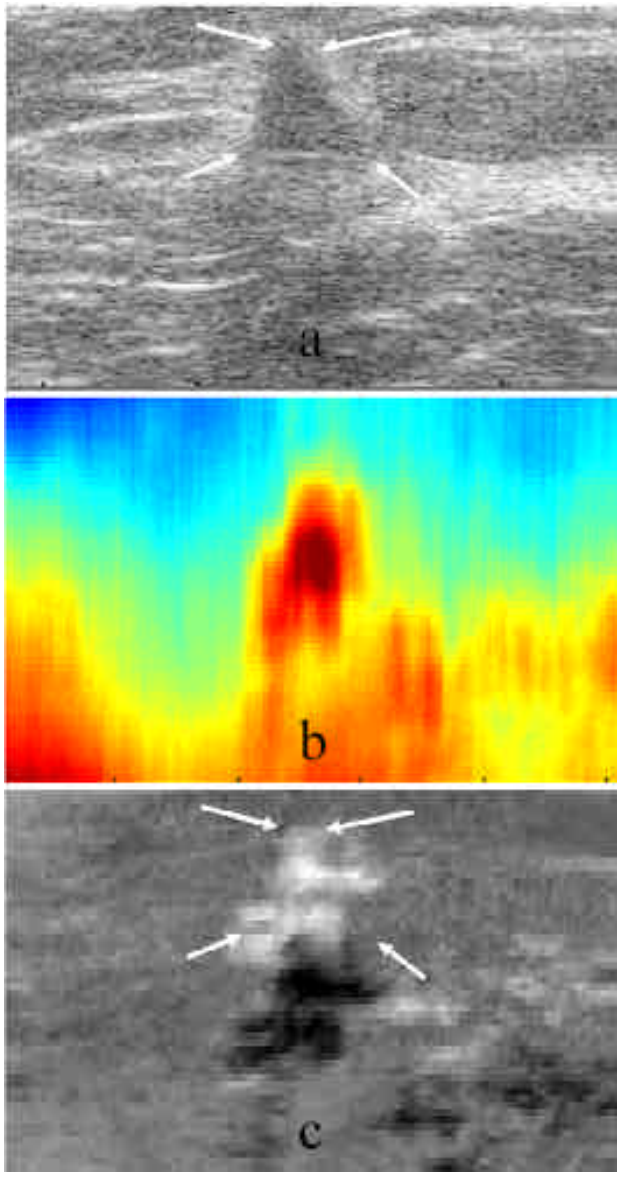


**Fig. (4).** Sonogram (a), displacement map (b) and elastogram (c) of a 10 mm IDC (48 years old patient). The displacement map shows a region of very high motion around the lesion. The lesion appears very bright (soft) on the elastogram.

These examples demonstrate that nonpalpable lesions as small as 10 mm may clearly show high contrast in strain images although the contrast can be of either polarity.

Fig. (**5a**) shows an example of a 10 mm IDC lesion. Although this lesion has the same triangular shape as the one on Fig. (**3a**), it was not detected by elasticity imaging. The elastogram (Fig. (**5c**)) does not exhibit any particular contrast around the lesion area and the displacement map (Fig. (**5b**)) does not show any clear disruption of the displacement slope.

Fig. (**6**) shows a 5 mm IDC lesion. Although the displacement map (Fig. (**6b**)) shows a decrease from left to right corresponding to tissue slipping that makes the interpretation more difficult, a bulge in the displacement

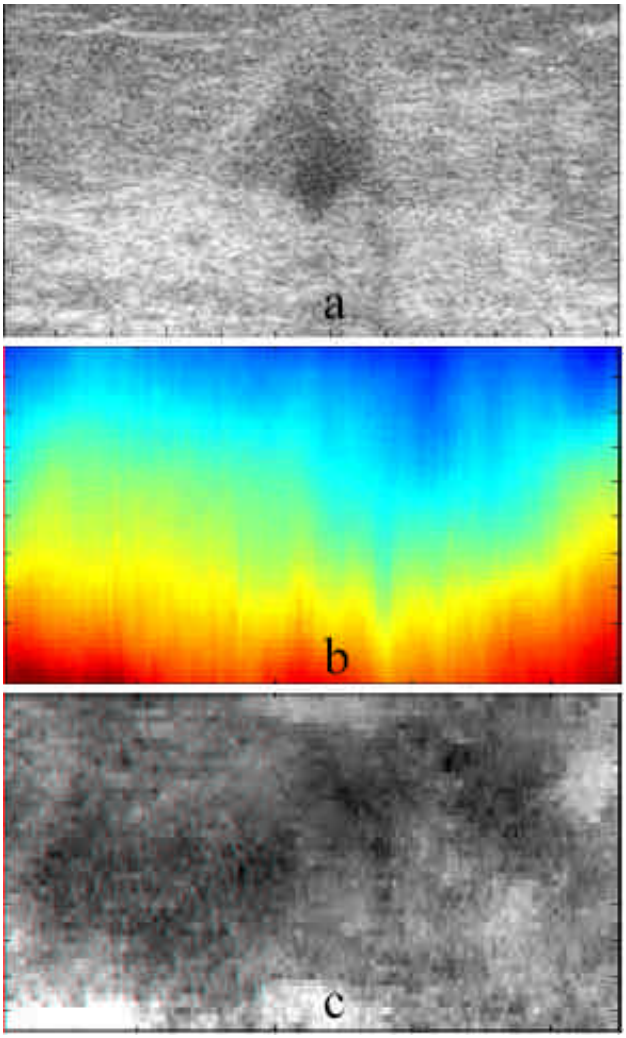


**Fig. (5).** Sonogram (a), displacement map (b) and elastogram (c) of a 10 mm IDC (83 years old patient). Neither the elastogram (Fig. 5c) nor the displacement map exhibit any particular contrast around the lesion area.

map near the lesion is clearly observed. This appears on the elastogram (Fig. (**6c**)) as a slightly darker region. For this small lesion, the displacement map alerts us of a suspected malignancy, even when elastogram findings are equivocal.

## IV- SUMMARY AND CONCLUSIONS

In this preliminary study, 6 benign lesions were studied and none appeared suspicious on elastograms (specificity of 6/6).

Among the 7 nonpalpable malignant lesions studied, the two lesions, of size 10 and 16 mm and depths 8 and 25 mm, were clearly distinct from their sounding tissues. The patients were, respectively, 48 and 66 years old. The two lesions were not at all alike; one lesion was very soft while the other one exhibited a stiff desmoplasic reaction.

Two other malignant lesions of size 6 and 10 mm and depth 18 and 12 mm, were not visible on the elastograms. The patients were, respectively, 46 and 83 years old. Our

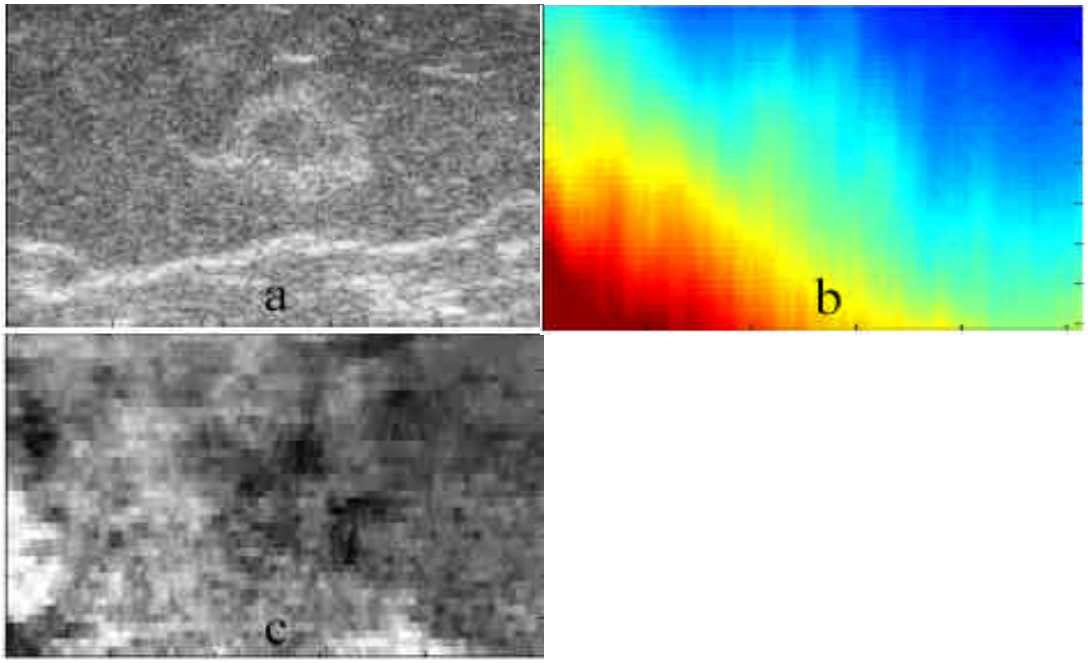


**Fig. (6).** Sonogram (a), displacement map (b) and elastogram (c) of a 5 mm IDC (53 years old patient). A bulge around the lesion is observed on the displacement map. The IDC is less clearly detected (less contrast) on the elastogram.

inability to detect the first lesion could be partly explained by its small size. The older patient had mostly fatty breast tissue that could affect our ability to compress the lesion in a manner that generates visible contrast. Average breast composition may be an important consideration when interpreting images for diagnosis.

The other 3 malignant lesions were not clearly identified as areas with extreme elasticity values, but exhibited suspicious patterns, especially in the displacement maps that showed bulges near the lesion. The lesions were respectively 5, 5 and 10 mm and the patient ages were 74, 53 and 81 years. The visibility of small lesions is limited by the spatial resolution of the imaging technique. The fatty replaced nature of the tissue of the 81 years old patient could be a factor limiting the elastic contrast for the third lesion. Keep in mind that this study concentrates on nonpalpable lesions, which are of great interest for detection and classification but pose the greatest challenge for elasticity imaging.

Although it would be premature to evaluate clinical utility of elasticity breast imaging or recommend techniques, these preliminary clinical studies suggest that lesion size and depth, resolution of the technique and breast composition must all be considered when interpreting images. We thus suggest the breast tissue be classified in the 4 density categories used in mammography (fatty replaced, scattered fibroglandular density, heterogeneously dense, dense) and interpreted accordingly. We also recommend observing the displacement map for confirmation of findings or highlighting of suspicious regions.

Inability to manually palpate a lesion does not obviously correlate with its elasticity image contrast. We did not study effects of lesion location, although our results show location can influence elasticity contrast, as some areas are easier to compress than others (for example when the chest wall can be used as a support). We also believe that interpretation criteria other than the relative elasticity, e.g., the change in strain with increasing compression, need to be investigated in order to improve the diagnostic capability of strain imaging.

This paper presents very preliminary results on a small number of subjects. These early findings on a particularly difficult patient population show however that elasticity imaging has the potential for discriminating benign from malignant nonpalpable lesions larger than 8 mm. Controlling for imaging effects with a well characterized imaging algorithm, allows us to have confidence that the elasticity images reflect tissue properties. This information complements mammography and sonography at little additional cost. While we cannot yet assess clinical utility, we have detected a large amount of tissue diversity in the population that suggests factors like lesion size, depth and breast composition must be taken into account before interpretation is possible. We are continuing to investigate the different issues that were raise in this study on a larger number of patients.

## ACKNOWLEDGEMENTS

The authors are very thankful to Pam Phelps at the UC Davis Medical Center for her help recruiting patient and acquiring data. They also gratefully acknowledge contributions from Patrick Von Behren, Levin Nock, and Shelby Brunke at Siemens Medical Solutions. This work was supported in part by grants from the National Institutes of Health R01 CA82497 and Siemens Medical Solutions, Ultrasound Group.

## REFERENCES

[1] American Cancer Society, 1599 Clifton Road NE, Atlanta GA. http: //www.cancer.org

[2] Humphrey LL, Helfand M, Chan BK, Woolf SH. Breast cancer screening: a summary of the evidence for the U.S. Preventive Services Task Force. Ann Intern Med.137(5 Part 1) 2002; 347-60.

[3] Barlow WE, Lehman CD, Zheng Y, *et al.* Performance of diagnostic mammography for women with signs or symptoms of breast cancer. J Natl Cancer Inst 2002; 94(15): 1151-9.

[4] Houssami N, Ciatto S, Irwig L, Simpson JM, Macaskill P. The comparative sensitivity of mammography and ultrasound in women with breast symptoms: an age_specific analysis. The Breast 2002; 11: 125-130.

[5] Elenbaas B, Weinberg RA. Heterotypic signaling between epithelial tumor cells and fibroblasts in carcinoma formation. Exp Cell Res 2001; 264: 169-84.

[6] Gilles RJ, Raghunand N, Karczmar GS, Bhujwalla ZM. MRI of the tumor microenviroment. J Mag Res Imag 2002; 16: 430-50.

[7] Chapman JD, Engelhardt EL, Stobbe CC, Schneider RF, Hanks GE. Measuring hypoxia and predicting tumor radioresistance with nuclear medicine assays. Radiother Oncol 1998; 46: 229-37.

[8] Contag CH, Ross BD. It's not just about anatomy: *in vivo* bioluminescence imaging as an eyepiece into biology. J Mag Res Imag 2002; 16: 378-87.

[9] Garra BS, Cespedes EI, Ophir J, Spratt SR, Zurbier RA, Magnant CM, Pannanen MF. Elastography of breast lesions: initial clinical results. Radiology 1997; 202: 79-86.

[10] Doyley MM, Bamber JC, Fuechsel F, Bush NL. A freehand elastographic imaging approach for clinical breast imaging: system development and performance evaluation. Ultrasound Med. Biol 2001; 27: 1347-1357.

[11] Hiltawsky KM, Kruger M, Starke C, Heuser L, Ermert H, Jensen A. Freehand ultrasound elastography of breast lesions: clinical results. Ultrasound Med. Biol 2001; 27(11): 1461-1469.

[12] Hall TJ, Zhu Y, Spalding CS. *In vivo* real-time freehand palpation imaging. Ultrasound Med. Biol 2003; 29(3): 427-435.

[13] McKnight AL, Kugel JL, Rossman PJ, Manduca A, Hartmann LC, Ehman RL. MR elastography of breast cancer: preliminary results. Am J Roentgenol 2002; 178: 1411-7.

[14] Lorenzen J, Sinkus R, Lorenzen M, *et al.* MR elastography of the breast: preliminary clinical results. Rofo Fortschr Geb Rontgenstr Neuen Bildgeb Verfahr 2002; 174: 830-4.

[15] Nightingale K, Soo MS, Nightingale R, Trahey G. Acoustic radiation force impulse imaging: *in vivo* demonstration of clinical feasibility. Ultrasound Med Biol 2002; 28: 227-35.

[16] Sandrin L, Tanter M, Catheline S, Fink M. Shear modulus imaging with 2-D transient elastography. IEEE Trans Ultrason Ferroelectr Freq Control 2002; 49(4): 426-35.

[17] Sridhar M, Pellot-Barakat C, Insana MF. Ultrasonic Mechanical Relaxation (UMR) Imaging, IEEE Ultrasonics Symp 2003; 929-932.

[18] Insana MF, Pellot-Barakat C, Sridhar M, Lindfors KK. Viscoelastic imaging of breast tumor microenvironment with ultrasound. J. Mamm. Gland Biol. Neoplasia 2004; 9: 393-404.

[19] Barsky SH, Rao CN, Grotendorst GR, Liotta LA. Increased content of Type V Collagen in desmoplasia of human breast carcinoma. Am J Pathol 1982; 108(3): 276-83.

[20] Pellot-Barakat C, Frouin F, Insana MF, Herment A. Ultrasound elastography based on multi-scale estimations of regularized displacement fields. IEEE Transactions on Medical Imaging 2004; 23 (2), 153-163.

[21] O'Donnell M, Skovoroda AR, Shapo BM, Emelianov SY. Internal displacement and strain imaging using ultrasonic speckle tracking. IEEE Trans Ultrason Ferroelec Freq Control 1994; 41: 314–325.

[22] Ophir J, Cespedes I, Ponnekanti H, Yazdi Y, Li X. Elastography: a quantitative method for imaging the elasticity of biological tissues. Ultrasonic Imaging 1991; 13: 111-34.

[23] Plewes DB, Bishop J, Samani A, Sciarretta J. Visualization and quantification of breast cancer biomechanical properties with MR elastography. Phys Med Biol 2000; 45: 1591-610.

[24] Yeung F, Levinson SF, Fu D, Parker KJ. Feature-adaptive motion tracking of ultrasound image sequences using a deformable mesh. IEEE Trans Med Imaging 1998; 17: 945-56.

[25] Sridhar M, Du H, Pellot-Barakat C, Tsou JK, Insana MF. Ultrasonic imaging of biochemical changes in tissues. Proc IEEE Ultrasonics Symp, August 2004.

[26] Ophir J, Garra BS, Kallel F, Konofagou EE, Krouskop TA, Righetti R, Varghese. T. Elastographic imaging. Ultrasound Med. Biol. 2000; 26: 23-29.

[27] Chaturvedi P, Insana MF, Hall TJ. 2-D companding for noise reduction in strain imaging. IEEE Trans. Ultrason. Ferroelectr. Freq. Control 1998; 45: 179-91.

[28] Pellot-Barakat C, Mai JJ, Kargel C, Herment A, Trummer B, Insana MF. Acce lerating Ultrasonic Strain Reconstructions by Introducing Mechanical Constraints. SPIE 2002; 4684: 323-333.

[29] Herment A, Pellot C, Giovannelli JF. Application of Regularization methods to cardiovascular imaging, In: Medical Image Processing: From pixel to structure, Ed. Ecole Polytechnique de Montreal 1997; 27-55.

[30] Pellot-Barakat C, Liu J, Frouin F, Herment A, Insana MF. Performance analysis of a regularized algorithm for elasticity imaging. IEEE Ultrasonics Symp 2003; 1622-1625.

[31] Varghese T, Ophir J, Cespedes I. Noise reduction in elastograms using temporal stretching with multicompression averaging. Ultrasound Med. Biol 1996; 22(8): 1043-52.

[32] Pepper Schedin, Anthony Elias. Multistep tumorigenesis and the microenvironment. Breast Cancer Res 2004; 6: 93-101.

[33] Mikala Egeblad, Zena Werb. New Functions for Matrix Metalloproteinases in Cancer Progression. Nature Reviews 2002; 161-174.

Received: March 04, 2005 Accepted: June 03, 2005